Lattice induced strong coupling and line narrowing of split resonances in metamaterials

Thomas CaiWei Tan [1,2,3], Yogesh Kumar Srivastava [1,2],

Manukumara Manjappa [1,2], Eric Plum [3] and Ranjan Singh [1,2,*]

[1]*Division of Physics and Applied Physics, School of Physical and Mathematical Sciences, Nanyang Technological University, Singapore 637371, Singapore*
[2]*Centre for Disruptive Photonic Technologies, The Photonics Institute, Nanyang Technological University, Singapore 637371, Singapore*
[3]*Centre for Photonic Metamaterials and Optoelectronics Research Centre, University of Southampton, Highfield, Southampton, SO17 1BJ, UK*
[*]Email: ranjans@ntu.edu.sg

Abstract

Strongly coupled metamaterial resonances typically undergo mode-splitting by which there is an exchange of energy between matter excitations and photons. Here, we report a strong coupling of the lattice mode with the structural eigen resonances of a split-ring metamaterial associated with mode-splitting and resonance line-narrowing that gives rise to high quality (*Q*) factor resonances. We demonstrate selective control of the resonance strength, line width and *Q*-factor of individual split-ring modes by tailoring the coupling of the fundamental lattice mode to each of the split-ring's hybridized resonances. A three-coupled-oscillator model shows lattice-mediated strong coupling in the form of an anti-crossing behavior between the hybridized metamaterial resonances. Such schemes of strong coupling between the lattice and the split hybrid modes of the metamaterial unit cell offer an avenue to invoke high-*Q* resonances and strong field confinement which could find applications in designing ultrasensitive sensors, multiband narrow filters, and slow light devices.

Metamaterials[1,2] are artificial structures engineered to display unique optical properties that are absent in natural materials, such as negative refraction[2,3], invisibility cloaking[4,5], perfect lensing[6,7], sensing functionalities[8] and phase compensation[9]. These artificially engineered materials are composed of so-called metamolecules of subwavelength size that are typically designed with high conductivity Drude metals structured in a periodic array. Due to their subwavelength periodicity, they interact homogenously with the incident electromagnetic field and can exhibit strongly resonant responses. Earlier studies have shown that different metamaterial resonances can be coupled to achieve narrow resonant features mimicking electromagnetically induced transparency (EIT)[10-14]. EIT type resonances in metamaterials involve nearfield coupling between superradiant "bright modes" and subradiant "dark modes". Bright modes are highly radiative and directly excited by the incident electric field, whereas dark modes, arise from asymmetric near field coupling of the metamaterial elements, they are weakly coupled to the incident field and trap electromagnetic energy within the resonator[15]. Similarly, metamaterial resonances could also be coupled to elementary excitations such as excitons[16] or phonons[17-19] to observe similar phenomena.

Since metamaterials are periodic structures with subwavelength lattice parameters, another class of dark modes exists in the array, the lattice modes. A lattice mode corresponds to diffraction along the interface of a periodic structure and mimics a surface plasmon polariton wave. Lattice modes are observed as kinks or discontinuities

in the transmission and reflection spectra of the metamaterial and they are also known as Woods anomalies[20]. The first order lattice mode (0,1) traps the diffracted field along the metal-dielectric interface of the periodic metamaterial array[21]. Due to the trapped fields, the lattice mode behaves like a dark mode and its resonant frequency can be easily controlled by changing the periodicity of the array. Coupling of the lattice mode to the eigenmodes of the metamaterial can lead to intriguing effects such as extraordinary transmission[22,23] and/or resonance line width narrowing[21,24] that give rise to extremely high quality (*Q*) factors. We note that control over *Q*-factor and depth of resonances have also been reported for three-dimensional metamaterials consisting of coupled resonators that can be tuned dynamically using MEMS approaches[25,26]. The lattice modes, that exist in any periodic array, allow linewidth and amplitude of resonances to be engineered while retaining the simplicity and low fabrication cost of planar metamaterials. High *Q*-factor devices minimize radiative losses and increase the sensitivity of the confined fields to external perturbation. These are characteristics needed in practical applications such as metamaterial spasers[27], sensors[8] and slow light devices[28].

In this work, we investigate the coupling between the fundamental lattice mode and the hybridized resonances of a terahertz asymmetric split-ring resonator (TASR) metamaterial array with the incident electric field polarized parallel to the gap arm. We demonstrate *Q*-factor enhancement of an individual hybrid mode when it is resonantly coupled to the lattice mode and disappearance of the mode-splitting associated with

decoupling of the lattice mode from the TASR eigenmodes. Hence, our results indicate that the mode splitting, also known as lattice induced transparency (LIT)[29], requires coupling of the lattice mode to the TASR eigenmodes. These eigenmodes are the antisymmetric resonance mode that is excited due to structural symmetry breaking and the symmetric resonance mode that is a broad dipole resonance occurring in both perfectly symmetric as well as asymmetric structures. Through this lattice mode coupling and a three-oscillator model, we show the existence of an anti-crossing behavior of the hybridized resonances that suggests a strong-coupling regime of the bright-lattice-dark (dipole-diffractive-asymmetric) mode interactions.

By varying the period *P* of the metamaterial unit cell, the frequency of the fundamental lattice mode can be tuned to couple to either of the two hybrid resonances. The frequencies of the lattice modes for a square lattice are given by

$$f_{LM} = \frac{c}{nP}\sqrt{i^2 + j^2} \quad (1)$$

where c is the speed of light in vacuum, n is the refractive index where the lattice mode propagates, P is the lattice period and (i,j) are non-negative integers defining the order of the lattice mode. In our study, we only consider coupling between the metamaterial resonances and the first-order lattice mode (0,1) that propagates in the substrate of our metamaterial, for which $f_{LM} = c/nP$.

Figure 1(a) shows the metamaterial array that consists of periodically arranged asymmetric split-ring resonators. The dimensions of the metamaterial's square unit cell

are depicted in the inset of Figure 1(b). The asymmetry, d = 8 μm, is introduced in the structure by moving one gap away from the central vertical axis and the period *P* of the unit cell is varied to tune the frequency of the lattice mode. The metamaterial samples were fabricated using photolithography with positive photoresist (AZ5214E) on a double side polished, high resistivity (> 5000 Ω-cm) silicon substrate of 500 μm thickness. A 200 nm thick aluminium layer was thermally evaporated over the patterned substrate and the undesired aluminium was lifted off using acetone. The fabricated metamaterial arrays have an overall size of 1 cm x 1 cm each and an optical microscope image of a small portion of an array is shown in Figure 1(b). The samples were characterized using photoconductive-antenna-based terahertz time domain spectroscopy (THz TDS) and the transmission amplitude was obtained by normalizing $|t(\omega)| = |E_S(\omega)/E_R(\omega)|$, where $E_S(\omega)$ and $E_R(\omega)$ are Fourier transforms of the electric field transmitted through the metamaterial sample and a reference substrate, respectively. The metamaterial samples were loaded on a sample holder with a circular aperture of 10 mm diameter and characterized by a THz beam of 5 mm diameter, which corresponds to 25% of the exposed metamaterial area, see Supplementary Figure S1. Depending on the metamaterial periodicity, the illuminated area corresponds to 1400 to 4000 resonators.

First, numerical investigations were performed using the CST Microwave Studio Frequency Domain Solver to understand the effect of the periodicity variation on the resonances of the TASR metamaterial. The aluminum split rings were modelled with a

DC conductivity of 3.56 x 10^7 S/m and the silicon substrate with a refractive index of $n = 3.42$. In the simulation, the periodicity *P* of the structure was varied from 70 μm to 120 μm to investigate the interaction of the first order lattice mode with the hybridized modes of the TASR. Figure 2 shows both simulated and measured transmission spectra, which are in good qualitative agreement. Quantitative deviations in the line-widths and amplitude of the resonances between the simulated and experimental results are mainly due to the low spectral resolution of the THz TDS setup. Deviations in the resonance frequencies of few percent are mainly due to fabrication imperfections. By increasing the period *P* from 70 μm to 120 μm, the spectral position of the first order lattice mode is varied to couple to the metamaterial resonances. Through this coupling, the split-ring resonances redshift, and their spectral linewidth changes. Mode splitting (mode hybridization) with an intermediate transmission peak is observed. The resonant transmission amplitude minima and maxima of the metamaterial are narrowest at critical periods, where the lattice mode resonantly couples with either of the hybrid modes (Figure 2(b) and (f)) or the transmission peak (Figure 2(c)). As the unit cell periodicity is increased above 90 μm, the mode-splitting disappears (Figure 2(g) and (h)). This indicates that coupling of the lattice mode to the metamaterial resonances in the TASR contributes to the hybridization of modes, which we address as the low frequency hybrid mode (LFHM) and the high frequency hybrid mode (HFHM). We note that the (1,1) order lattice mode can be seen for periodicities of 90 μm and 120 μm at frequencies of 1.38 THz and 1.03 THz, respectively (Figure 2(g) and 2(h)).

As the lattice mode is swept across the metamaterial resonances, drastic changes occur in the linewidths and the resonance intensity of the LFHM, the HFHM and the LIT transmission peak in between. Figure 3 shows the *Q*-factor ($Q = f_0/\Delta f$) of the HFHM and the LFHM as a function of the lattice period, which is calculated from the transmission intensity $|t(\omega)|^2$, where f_0 is the resonance frequency and Δf is the line width measured as full width at half maximum (FWHM) of the resonance in the transmission intensity spectrum. As the lattice mode is swept across the HFHM resonance by increasing the lattice period from 65 μm to 82 μm, the *Q*-factor of the HFHM decreases gradually from 31 to 6, see Figure 3(a). As the lattice mode frequency falls below the HFHM, the HFHM resonance broadens and the associated transmission increases. The resonant change in transmission becomes small at larger periodicities, see Figure 2. This could be due to decoupling from the lattice mode and a weaker collective response from the larger unit cells in the metamaterial structure[30,31]. On the other hand, as the lattice period is increased such that the lattice mode frequency approaches the LFHM, there is an exponential increase in its *Q*-factor, as shown in Figure 3(b). This exponential increase is due to the gradual increase in coupling of the lattice mode to the LFHM that confines the electromagnetic energy in the metamaterial array. At *P* = 87 μm, where the lattice mode resonantly couples with the LFHM, the *Q*-factor reaches 113 which is an order of magnitude higher than the HFHM of the same structure. In this case, both narrowing and reduced depth of the transmission resonance contribute to the observed exponential increase in the *Q*-factor. The practical

importance of tailoring the *Q*-factors is apparent in terms of a figure of merit (FoM), which also considers the strength of the resonance and is useful for designing efficient sensors and nonlinear devices. The figure of merit ($FoM = Q \times \Delta I$) is defined as the product of *Q*-factor and change in transmission intensity ΔI (depth) of the resonance spectra. Figures 3(c) and 3(d) show the FoM for the HFHM and LFHM resonances, which reach maxima of 11 and 19, respectively. Like its *Q*-factor, the FoM of the HFHM is largest at smaller periods. As the period increases from 65 μm to 87 μm, it drops by an order of magnitude due to the broadening of the resonance, the increase in resonant transmission intensity and the vanishing of the neighboring LIT transmission peak at larger lattice periods. In the case of the LFHM, not only the *Q*-factor but also the FoM shows an exponential increase, which reaches a maximum FoM of 19 and *Q*-factor of 113 at *P* = 87 μm. At this period, the LFHM provides higher sensitivity and lower radiative losses due to the strong coupling with the lattice mode that enhances the confined near field energy in the split-ring gap.

Further investigation of the electric field confinement and surface currents of the lattice matched hybrid modes (*P* = 75 and 87 μm) is shown in Figure 4. Little electric field confinement was seen in both hybrid modes at *P* = 75 μm as the surface currents remain in a dipole configuration which is highly radiative. However, at *P* = 87 μm, when the lattice mode frequency closely matches the LFHM, the surface currents are in a quadrupole configuration resulting in strong electric field confinement and a high *Q*-factor of 113 (Figure 4b, *P* = 87 μm, left). Another point to note is that as the first order

lattice mode crosses the LFHM, the surface currents and field distribution of the HFHM show a dipole configuration (Figure 4b, P = 87 μm, right), which corresponds to a broad minimum in transmission. Interestingly, for periods larger than 87 μm, the mode-splitting is barely visible in the spectrum (Figure 2), suggesting that the fundamental lattice mode decouples from the TASR eigenmodes and mode-splitting switches off. This investigation indicates the role of the first order lattice mode in the mode-splitting effect in the system. However, our structure also possesses a structural asymmetry that contributes to the observed mode-splitting. Therefore, a similar investigation was performed with a symmetric resonator (symmetric gap, d = 0) of otherwise same dimensions. No mode splitting was observed in the symmetric structure even under lattice matched conditions, as shown in Supplementary Figure S2. Hence, our results show that the mode-splitting effect occurs under two conditions. First, the metamaterial resonator must be asymmetric, and second, the fundamental lattice mode must be close to the structural resonance of the metamaterial resonator.

As the lattice mode is swept across the hybrid modes, not only the amplitude and width but also the spectral position of the resonances changes. The observed periodicity-dependence of the two hybrid mode frequencies reveals an anti-crossing behavior, which is a signature of a strongly coupled system. We modelled this coupling with a three-oscillator model[29,32-34], which is described in detail in the supplementary material. Its oscillators correspond to the symmetric bright mode, the lattice mode and the asymmetric dark mode which arises due to the structural symmetry breaking. The

coupled equations representing the interaction between the bright, lattice and dark modes are expressed as

$$(-\omega^2 - i\omega\gamma_b + \omega_b^2)\tilde{x}_b + \Omega_1^2\tilde{x}_{LM} = \tilde{E}(\omega) \quad (2a)$$

$$(-\omega^2 - i\omega\gamma_{LM} + \omega_{LM}^2)\tilde{x}_{LM} + \Omega_1^2\tilde{x}_b - \Omega_2^2\tilde{x}_d = 0 \quad (2b)$$

$$(-\omega^2 - i\omega\gamma_d + \omega_d^2)\tilde{x}_d + \Omega_2^2\tilde{x}_{LM} = 0 \quad (2c)$$

where $(\tilde{x}_b, \tilde{x}_{LM}, \tilde{x}_d), (\omega_b, \omega_{LM}, \omega_d)$ and $(\gamma_b, \gamma_{LM}, \gamma_d)$ are the displacement amplitudes, resonance angular frequencies, and damping rates of the bright mode, lattice mode and dark mode respectively. Ω_1 and Ω_2 are the bright-lattice and dark-lattice mode coupling strengths, respectively. In this model, the lattice mode mediates the coupling between the bright and dark modes. Equation (2a) is the equation of motion for the bright mode and it is driven by the incident light, while (2c) is the equation of motion of the dark mode of the TASR, and they are both coupled to the lattice equation of motion (2b) by the coupling strengths Ω_1 and Ω_2 respectively.

The bright mode frequency of 1.1 THz is taken as the dipole frequency of a symmetric split-ring resonator, whereas ω_{LM} is obtained from the simplified expression of Equation (1). Also w_d is taken to be equal to ω_{LM} as the lattice mode mediates the coupling of the dark mode to the bright mode in our model. Based on the linewidths, the damping rates were taken as $\gamma_b = 10^{12}$ rad/s and $\gamma_{LM} = \gamma_d = 0.15 \times 10^{12}$ rad/s while Ω_1 and Ω_2 are taken as free parameters. With this model, the eigenvalues of the coupled equations are solved through the diagonalization of matrix M:

$$M = \begin{pmatrix} \Lambda_b & \Omega_1^2 & 0 \\ \Omega_1^2 & \Lambda_{LM} & -\Omega_2^2 \\ 0 & \Omega_2^2 & \Lambda_d \end{pmatrix} \quad (3)$$

where $\Lambda_i = -\omega^2 - i\omega\gamma_i + \omega_i^2$ and $i = b, LM, d$. The eigenvalues of the diagonalized matrix are the two hybrid modes of the coupled system and the lattice mode. A numerical fitting was performed to obtain the best values to fit the simulations, resulting in $\Omega_1 = 2.30 \times 10^{12}$ rad/s and $\Omega_2 = 1.84 \times 10^{12}$ rad/s. As illustrated in Figure 5, the three-oscillator model (red circles) fits the simulations (green squares) well at larger periodicities. But the oscillator model does not account for the nearest neighbor coupling of the metamaterial unit cells, resulting in deviations at smaller periodicities, where the simulated resonance shift of the HFHM is less prominent than predicted by the analytical model. Figure 5 also shows the crossing of the period-dependent lattice mode and the bright dipole mode at 1.1 THz. This crossing corresponds to the high-*Q* lattice induced transparency peak shown in Figure 2(c). In this system, the lattice mode mediates the coupling of the bright mode to the dark mode, giving rise to the observed anti-crossing. Therefore, this anti-crossing behavior alongside the coupling strength where $\Omega > \gamma$ is a signature of a strongly coupled system that can only be observed at periodicities P < 90 μm as the mode-splitting vanishes at larger periodicities.

In summary, we demonstrated how lattice modes can be used to control the strength and width of hybridized resonances in metamaterial arrays of asymmetric resonators. By varying the metamaterial periodicity, we selectively coupled the fundamental lattice

mode to either of the hybridized modes of terahertz asymmetric split-ring resonators and were able to tune the resonance *Q*-factor of one hybrid mode from 5 to 113. We have also reported evidence of strong coupling between the bright, lattice and dark modes in the form of an anti-crossing behavior using a three-oscillator model. This simple approach of in-plane coupling of the fundamental lattice mode and metamaterial resonances can be used as an efficient technique to optimize metamaterial designs to reduce radiative losses and to provide high-*Q* resonances for practical applications such as ultrasensitive sensors and low threshold lasing spasers.

Supplementary Material

See supplementary material for the transmission spectra of the symmetric resonators and detailed information on the coupled oscillator model.

Acknowledgement

The authors acknowledge research funding support from the Singapore National Research Foundation (NRF), the French National Research Agency (ANR, grant NRF2016-NRF-ANR004) and the UK's Engineering and Physical Sciences Research Council (EPSRC, grant EP/M009122/1). Following a period of embargo, the data from this paper will be available from the University of Southampton ePrints research repository: http://doi.org/10.5258/SOTON/D0397

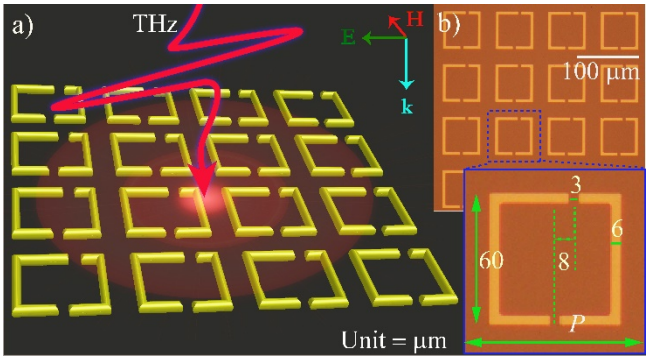

Figure 1: (a) Schematic illustration of the TASR metamaterial array, which is illuminated by a THz beam of 5 mm diameter. (b) Optical microscope image of the fabricated metamaterial array, with its unit cell dimensions shown in the inset. *P* is the periodicity of the unit cell which is a variable parameter in this investigation. All unit cell dimensions are given in micrometers.

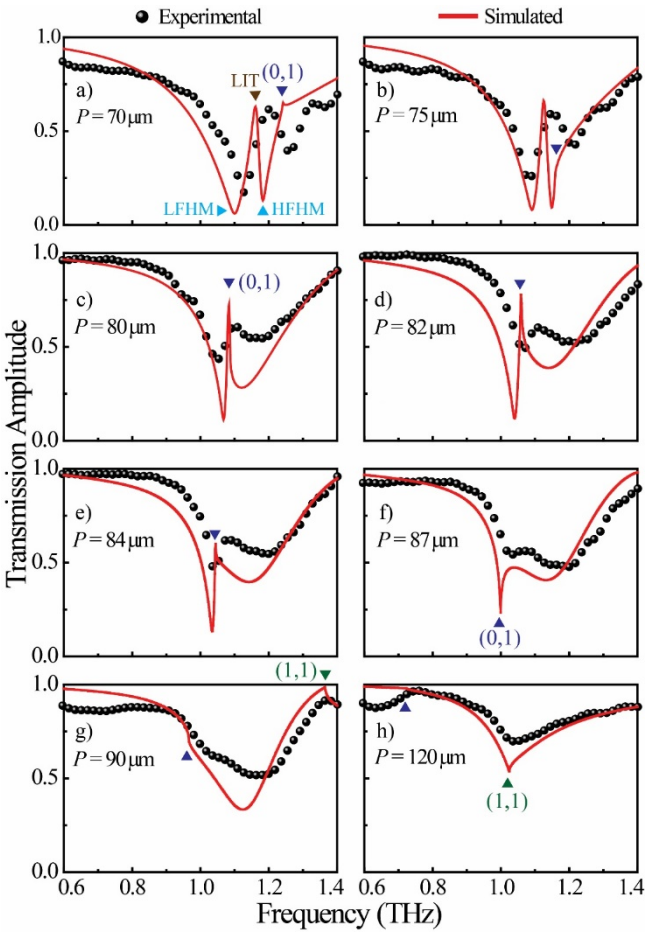

Figure 2: (a)-(h) Experimental (black spheres) and simulated (red solid lines) transmission amplitude of the TASR metamaterial array with varying lattice period P = 70, 75, 80, 82, 84, 87, 90 and 120 μm, respectively. The low frequency hybrid mode (LFHM) and high frequency hybrid mode (HFHM) are indicated in (a) and arise from the lattice induced transparency (LIT). The fundamental lattice mode (0,1) is indicated by a dark blue triangle and the (1,1) order lattice mode is indicated by a green triangle.

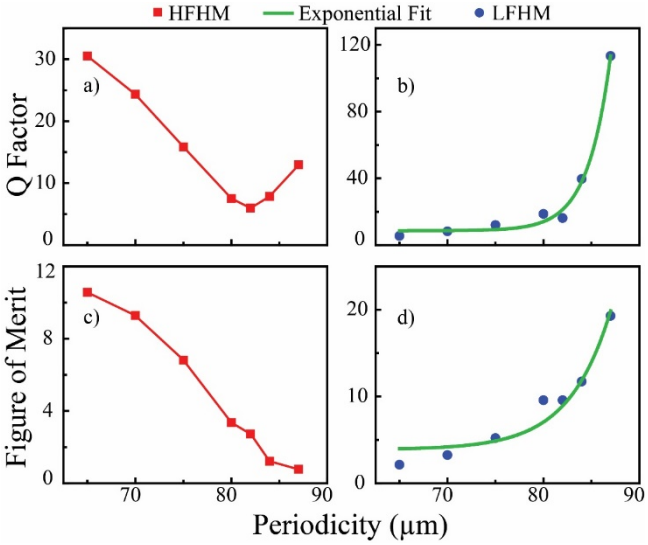

Figure 3. *Q*-Factor and figure of merit (FoM) of the HFHM and LFHM of the asymmetric metamaterial for different periodicities: (a, b) *Q*-factors of the HFHM and LFHM reaching a maximum of 31 and 113, respectively. (c, d) FoM of the HFHM and LFHM reaching a maximum of 11 and 19 respectively.

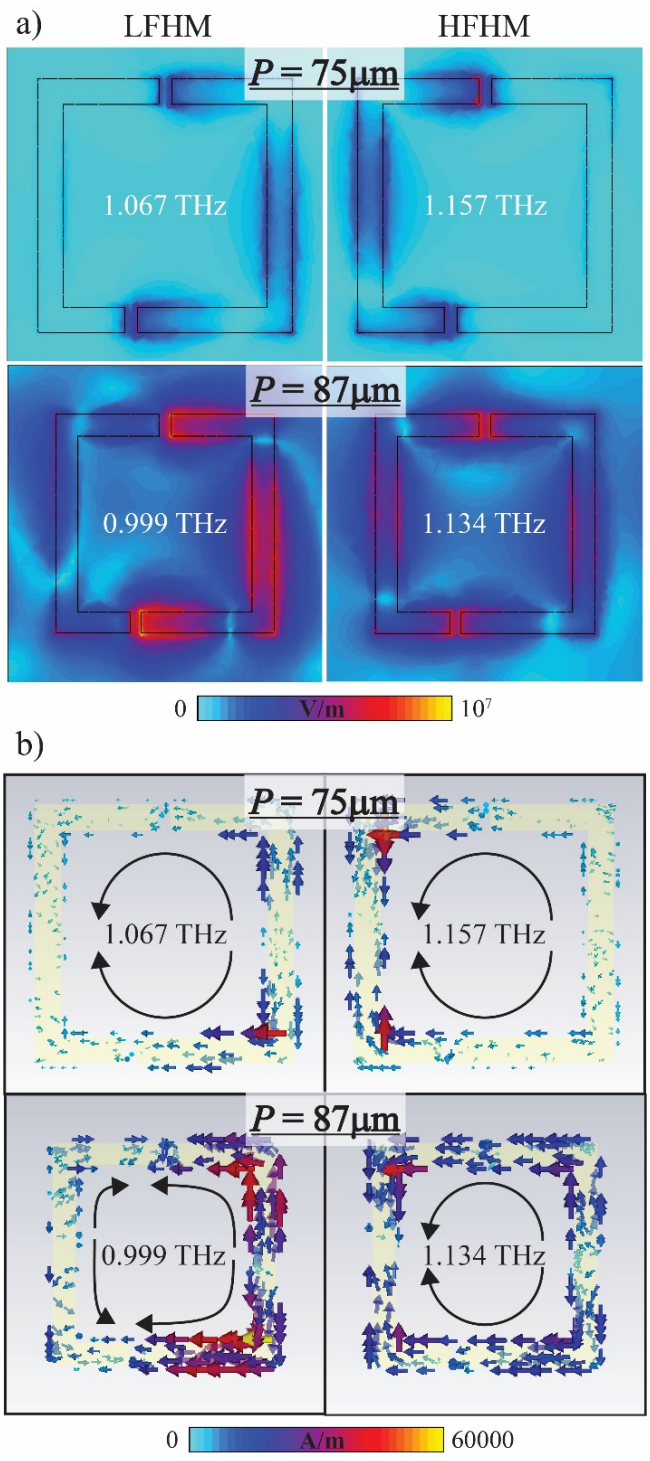

Figure 4: Distributions of (a) electric field magnitude and (b) surface currents of the LFHM and HFHM for metamaterial periods of 75 and 87 μm. For P = 75 μm the lattice mode is close to the HFHM and for P = 87 μm the lattice mode is close to the LFHM. The LFHM for period 87 μm is a quadrupole mode with high field enhancement while the others are electric dipole modes.

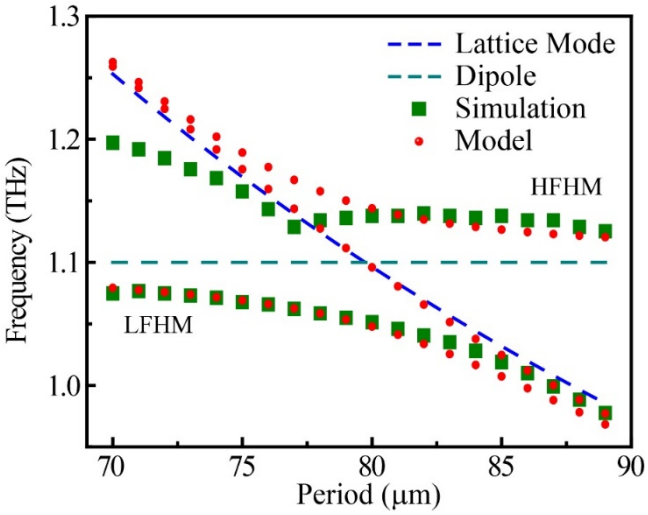

Figure 5: Resonance frequency of hybrid modes (LFHM and HFHM) and lattice mode with varying period of the metamaterial array according to simulations and analytical model. Anti-crossing behavior is seen at the intersection of the Dipole mode of 1.1 THz (cyan dash) and the calculated lattice mode according to Equation (1) (blue dash). The green squares represent the two hybrid split-ring modes from the simulation. The red circles represent the analytical eigensolution of the three-oscillator model.

Reference

[1] J. B. Pendry, A. J. Holden, D. J. Robbins, and W. J. Stewart, IEEE Transactions on Microwave Theory and Techniques **47** (11), 2075 (1999).

[2] D. R. Smith, J. B. Pendry, and M. C. K. Wiltshire, Science **305** (5685), 788 (2004).

[3] D. R. Smith, Willie J. Padilla, D. C. Vier, S. C. Nemat-Nasser, and S. Schultz, Phys. Rev. Lett. **84**, 4184 (2000).

[4] J. B. Pendry, D. Schurig, and D. R. Smith, Science **312** (5781), 1780 (2006).

[5] D. Schurig, J. J. Mock, B. J. Justice, S. A. Cummer, J. B. Pendry, A. F. Starr, and D. R. Smith, Science **314** (5801), 977 (2006).

[6] Nicholas Fang, Hyesog Lee, Cheng Sun, and Xiang Zhang, Science **308** (5721), 534 (2005).

[7] J. B. Pendry, Phys. Rev. Lett. **85**, 3966 (2000).

[8] Basudev Lahiri, Ali Z. Khokhar, Richard M. De La Rue, Scott G. McMeekin, and Nigel P. Johnson, Opt. Express **17** (2), 1107 (2009).

[9] Babak Dastmalchi, Philippe Tassin, Thomas Koschny, and Costas M. Soukoulis, Physical Review B **89** (11), 115123 (2014).

[10] Arif E. Çetin, Alp Artar, Mustafa Turkmen, Ahmet Ali Yanik, and Hatice Altug, Opt. Express **19** (23), 22607 (2011).

[11] Na Liu, Lutz Langguth, Thomas Weiss, Jurgen Kastel, Michael Fleischhauer, Tilman Pfau, and Harald Giessen, Nat Mater **8** (9), 758 (2009).

[12] Na Liu, Thomas Weiss, Martin Mesch, Lutz Langguth, Ulrike Eigenthaler, Michael Hirscher, Carsten Sönnichsen, and Harald Giessen, Nano Letters **10** (4), 1103 (2010).

[13] N. Papasimakis, V. A. Fedotov, N. I. Zheludev, and S. L. Prosvirnin, Physical Review Letters **101** (25), 253903 (2008).

[14] P. Tassin, Lei Zhang, Th Koschny, E. N. Economou, and C. M. Soukoulis, Physical Review Letters **102** (5), 053901 (2009).

[15] Shuang Zhang, Dentcho A. Genov, Yuan Wang, Ming Liu, and Xiang Zhang, Physical Review Letters **101** (4), 047401 (2008).

[16] P. Vasa, R. Pomraenke, S. Schwieger, Yu I. Mazur, Vas Kunets, P. Srinivasan, E. Johnson, J. E. Kihm, D. S. Kim, E. Runge, G. Salamo, and C. Lienau, Physical Review Letters **101** (11), 116801 (2008).

[17] Frank Neubrech, Annemarie Pucci, Thomas Walter Cornelius, Shafqat Karim, Aitzol García-Etxarri, and Javier Aizpurua, Physical Review Letters **101** (15), 157403 (2008).

[18] Frank Neubrech, Daniel Weber, Dominik Enders, Tadaaki Nagao, and Annemarie Pucci, The Journal of Physical Chemistry C **114** (16), 7299 (2010).

[19] D. J. Shelton, I. Brener, J. C. Ginn, M. B. Sinclair, D. W. Peters, K. R. Coffey, and G. D. Boreman, Nano Letters **11** (5), 2104 (2011).

[20] R. W. Wood, Philosophical Magazine **4** (21), 396 (1902).

[21] Andreas Bitzer, Jan Wallauer, Hanspeter Helm, Hannes Merbold, Thomas

Feurer, and Markus Walther, Opt. Express **17** (24), 22108 (2009).
22 Pernille Klarskov, Abebe T. Tarekegne, Krzysztof Iwaszczuk, X. C. Zhang, and Peter Uhd Jepsen, **6**, 37738 (2016).
23 Alexei Halpin, Niels van Hoof, Arkabrata Bhattacharya, Christiaan Mennes, and Jaime Gomez Rivas, Physical Review B **96** (8), 085110 (2017).
24 Janine Keller, Curdin Maissen, Johannes Haase, Gian Lorenzo Paravicini-Bagliani, Federico Valmorra, José Palomo, Juliette Mangeney, Jérôme Tignon, Sukhdeep S. Dhillon, Giacomo Scalari, and Jérôme Faist, Advanced Optical Materials **5** (6), 1600884 (2017).
25 G. R. Keiser, H. R. Seren, A. C. Strikwerda, X. Zhang, and R. D. Averitt, Applied Physics Letters **105** (8), 081112 (2014).
26 Xiaoguang Zhao, Kebin Fan, Jingdi Zhang, George R. Keiser, Guangwu Duan, Richard D. Averitt, and Xin Zhang, Microsystems &Amp; Nanoengineering **2**, 16025 (2016).
27 N. I. Zheludev, S. L. Prosvirnin, N. Papasimakis, and V. A. Fedotov, Nat Photon **2** (6), 351 (2008).
28 Martijn C. Schaafsma, Arkabrata Bhattacharya, and Jaime Gómez Rivas, ACS Photonics **3** (9), 1596 (2016).
29 Manukumara Manjappa, Yogesh Kumar Srivastava, and Ranjan Singh, Physical Review B **94** (16), 161103 (2016).
30 V. A. Fedotov, N. Papasimakis, E. Plum, A. Bitzer, M. Walther, P. Kuo, D. P. Tsai, and N. I. Zheludev, Physical Review Letters **104** (22), 223901 (2010).
31 Ranjan Singh, Carsten Rockstuhl, and Weili Zhang, Applied Physics Letters **97** (24), 241108 (2010).
32 Lukas Novotny, American Journal of Physics **78** (11), 1199 (2010).
33 Hua Xu, Yuehui Lu, YoungPak Lee, and Byoung Seung Ham, Opt. Express **18** (17), 17736 (2010).
34 Ningning Xu, Manukumara Manjappa, Ranjan Singh, and Weili Zhang, Advanced Optical Materials **4** (8), 1179 (2016).